Laboratory simulations of tensile fracture development in a volcanic conduit via cyclic magma pressurisation

Philip M Benson[1,2*], Michael J Heap[3], Yan Lavallee[4], Asher Flaws[4], K.-U. Hess[4], A.P.S. Selvadurai[5], Donald B Dingwell[4] and B. Schillinger[6]

[1] Geological Institute, Dept. Earth Sciences, Swiss Federal Institute of Technology, Zurich, 8092, Switzerland

[2] Rock Mechanics Laboratory, School of Earth and Environment, University of Portsmouth, Portsmouth, PO1 3QL, UK

[3] Laboratoire de Géophysique Expérimentale, Institut de Physique de Globe de Strasbourg (UMR 7516 CNRS, Université de Strasbourg/EOST), 5 rue René Descartes, 67084 Strasbourg cedex, France.

[4] Earth and Environment, LMU – University of Munich, Theresienstr. 41/III, 80333 München, Germany.

[5] Department of Civil Engineering and Applied Mechanics, McGill University, Montreal, Quebec, H3A 3K6, Canada.

[6] Forschungsreaktor FRM-II, Technische Universität München, 85747 Garching, Germany

* Corresponding Author: p.benson@ucl.ac.uk

Abstract

During volcanic unrest, high magma pressure induces cracking and faulting of the country rock, providing conduits for the transport of magma and other fluids. These conduits, known as dykes, are fundamental structures for the transport of magma to the surface in volcanically active regions. The mechanics of dyke propagation is not yet fully understood but is crucial to better model dyke emplacement and eruption in volcanoes. Central to this need is a greater understanding of the mechanical properties of the magma / country rock interaction as a function of known magmatic pressure, temperature and stress. Here, we report data from a series of experiments in which we cyclically compress viscoelastic rhyolitic magma (at 828 °C, 892 °C and 918 °C) inside a cylindrical conduit-like shell of basalt (from Mt. Etna, Italy) until fracture occurs. The compression is performed under strain rates cyclically varying between $5x10^{-6}$ and $5x10^{-5}$ s^{-1}. The resultant monitored (axial) loading and relaxation illustrates how the presence of a visco-elastic fluid (magma) controls the stress induced at the conduit margin boundary. This is achieved by analysing the viscoelastic relaxation (through time) to calculate an apparent modulus, which is found to decrease with both increasing temperature and time. In the 4 cycles before failure we find that the apparent modulus decreases from 180 to 40 GPa, 80 to 20 GPa and 8 to 1 GPa for imposed stress cycles at 828 °C, 892 °C and 918 °C, respectively. We theoretically estimate a tensile strength at failure of approximately 7 to 11 MPa, consistent with recent field data and in agreement with a model derived from the sample geometry and basic material parameters. Post-experimental neutron computed tomography and microscopic analyses further reveal the fragmentation of the melt and generation of tuffisite veins inside the conduit due to spontaneous crack nucleation associated with conduit wall fracture. The geometry of the rupture area inside the melt is akin to a Mach cone associated with supershear fractures. We discuss our findings in terms of magma-rock interaction leading to dykes, tuffisite veins and magma fragmentation.

Keywords: fracture nucleation, dyke propagation, magma fragmentation, tuffisite, supershear, Mach cone

1. Introduction

The link between magmatism and tectonic structures has long been recognised (e.g. Nakamura, 1977; De Natale et al., 1997; Acocella et al., 2001; Lavallée et al., 2009; Gudmundsson, 2011a). For instance, pressure gradients force magma to ascend through the crust via the process of tensile failure in the country rock at the propagating dyke tip, aided by any existing faults and fractures (Pitcher, 1979). Movement into and through these pathways produces stress fluctuations that act against the host rock and the local/regional tectonic stress field (Hutton, 1996). If the local strength of the rock is exceeded, the resultant failure will modify the stress field (Pertsov et al., 1977; Bonafede and Danesi, 2010), with repercussions on the chemical equilibrium of the magma under the new pressure conditions as well as creating new pathways to divert its course of ascent and to transport exsolved gases. Therefore, dyking exerts a primary control on the integrity of the host rocks whilst simultaneously affecting the physical and chemical evolution of the magma as it attempts to reach the surface and erupt. It follows that our assessments of volcanic hazards fundamentally rely on our knowledge of host rock failure, dyke injection and magma transport – processes controlled by the mechanical properties of the rock and the rheological behaviour of the intruding magma (e.g. Gudmundsson, 2011a).

The failure of rocks is initiated largely in tension (Griffith, 1920), owing to the tensile strength of rocks being approximately a tenth of their compressive strength (Jaeger and Cook, 2007). Shear faulting is essentially a result of the linkage of many smaller tensile cracks (e.g. Paterson and Wong, 2005). Once nucleated, fractures can further propagate due to perturbation of the elastic energy release rate or the stress intensity factor at the crack tips (Inglis, 1913; Broek, 1982). In the case of dyke propagation at high temperatures, the viscoelastic response of the rock, creep (subcritical crack growth) at the dyke tips may accelerate the propagation by one order of magnitude (Chen and Jin, 2011). Experimental

88 studies have mapped out the fracture toughness of volcanic rocks subjected to a range of
89 temperatures and confining pressures (Rocchi et al., 2004; Balme et al., 2004; Smith et al.,
90 2009). These findings therefore suggest that the propagation of tensile fractures would ease as
91 they extend towards the Earth's surface, a scenario usually favoured in numerical simulations
92 (e.g. Santoni et al., 2011). Although this result can be explained by reference to the classical
93 Griffith energy balance scenario it is important to also acknowledge that, on the other hand,
94 discontinuities are more likely to be open near to the surface leading to the Cook-Gordon
95 analysis of crack arrest (Gudmundsson, 2009). In the volcanic context, magma can more
96 easily infiltrate tensile fractures as seen in sheet-like dike structures with evidence of elastic
97 wall deformation (e.g. Cuevas et al., 2006). Field and theoretical studies have, however,
98 shown that the majority of dykes are arrested at depth (Gudmundsson and Brenner, 2001;
99 2004). In the Campi Flegrei caldera (Naples, Italy), for example, very few dykes are exposed
100 at the surface due to the soft overburden (e.g. De Natale et al., 1997), creating stress-release
101 barriers that adversely influence the ability of the dyke tip to propagate further
102 (Gudmundsson, 2011a). The source of these discrepancies may partly reside in the stress
103 imparted by the magma.
104
105 During ascent, the physical, chemical and thus rheological properties of magma evolve
106 (Sparks et al., 1997). Changes in pressure and temperature force crystallization and the
107 exsolution of volatiles which promote an increase in viscosity (Hess and Dingwell, 1996;
108 Lejeune and Richet, 1995) as well as an increase in pore pressure (Massol and Jappart, 1999).
109 These end effects counteract one another during the magma-driven fracture propagation
110 through the crust (Carrigan, 2000), an increase in viscosity serves to slow magma migration,
111 whereas an increase in pore fluid pressure favours cracking of the host rock. In addition,
112 bubble segregation from the magma followed by accumulation near the fracture tip can
113 amplify the local stress to exceed the fracture toughness. The relationship between the magma
114 rheology, the rock strength and the stress field generated at their interface is thus fundamental
115 to our understanding of fracturing, dyking and magma transport.

Experimental investigations of fracturing, dyking and magma transport are scarce. Work has concentrated either on analogue setups using gelatine and other materials that are fractured by injection of coloured water (Menand and Tait, 2001; Acocella et al., 2001; Walter and Troll, 2003), or – for simulation of representative rock properties – a simplified experimental setup at room temperatures. In the latter case, hydrofracturing is caused by increasing the water pressure within an axial conduit (cored out of a cylindrical rock shell) flanked by a rubber membrane (to isolate the fluid from the rock) until failure of the rock shell (e.g. Vinciguerra et al., 2004). Although useful for visualising the physical processes occurring during dynamic fracturing, this type of experiment cannot reveal the interaction between the dyke tip and the host rock because the pressurizing medium is mechanically coupled to the inner bore by the membrane. In addition, since this type of experiment is conducted at low temperatures, it cannot reproduce the behaviour of magma interacting with the host rock. Here, we experimentally simulate magma-rock interaction by compressing a magma inside a conduit-like cylindrical shell until fracturing of the shell occurs. The experiments provide an estimate of the magma stress relaxation and the tensile strength of the conduit wall rocks at high temperatures, as well as a description of the physics occurring at the onset of dyking.

2. Methods

Magma-rock failure tests were performed by combining Cougar Creek obsidian, CO, (from the Cougar Creek lava flow, Yellowstone National Park, USA; see Christiansen, 2001), and Etna basalt, EB, (from Mt. Etna volcano, Italy) in an experimental setup analogous to hydraulic fracture experiments (see below for details). The selected obsidian is a dense (porosity of < 0.1 %), aphyric rhyolite, simulating flow of a single-phase silicate melt at high temperature. The basalt is a porphyritic, alkali basalt of approximately 3.8% porosity. It comprises millimetre-size phenocrysts of pyroxene, olivine and feldspar within a fully

144 crystallized, fine-grained groundmass. The basalt was chosen because it has been extensively
145 studied (Stanchits et al., 2006; Benson et al., 2007; 2010; Heap et al., 2009; 2011) and
146 because its properties are nearly isotropic (e.g. ultrasonic wave velocities) and temperature
147 independent (the mechanical strength was found to be independent of temperature up to 900
148 °C). Furthermore, this basalt contains no glass, so it should not undergo softening at the
149 investigated temperatures. Thus, these materials were selected since the rhyolite can deform
150 viscously while the basalt will remain brittle under the given experimental temperatures. Our
151 study was carried out in three phases.
152
153 Firstly, we characterized the viscosity-temperature relationship of the rhyolitic melt to
154 be used as a guide for our experimental temperatures. We employed the standard
155 micropenetration technique using a Baehr vertical dilatometer, which involved monitoring the
156 penetration rate of an indenter (of known geometrical end shape) into a disc of melt (Hess and
157 Dingwell, 1996). The rate of indentation of a small melt disc (6 mm in diameter and 3 mm in
158 thickness) was used to compute the viscosity as a function of temperature, according to:
159
160 (1)
161
162 where F is the force applied by the indenter, t the time of indentation, r the indenter radius,
163 and α the indented depth. This method resolves the viscosity to within +/- 0.05 log unit of
164 viscosity (Hess and Dingwell, 1996).
165
166 Secondly, the uniaxial compressive strength of the basalt was investigated at a range of
167 temperatures (25, 200, 500, 750, 900 and 950 °C) on cylindrical cores (25 mm in diameter
168 and 75 mm in length) in a high-temperature uniaxial press (a full description of the uniaxial
169 press can be found in Hess et al., 2007). The strength tests were performed under the same
170 variable strain rates as used in the magma-rock failure tests (see below).

171

172 Finally, magma-rock failure tests were performed in the high-temperature uniaxial press
173 by pressing a plug of basalt (a disc 10 mm in diameter and 10 mm in length) onto a central
174 core of rhyolitic melt (10 mm in diameter and 85 mm in length) encased by an outer shell of
175 basalt (60 mm in diameter and 90 mm in length; Fig. 1). The plug of basalt ensured that the
176 inner conduit could be loaded without the loss of melt. Pressurisation of the inner melt was
177 achieved by cyclically changing the imposed axial strain rate between 3.2×10^{-5} s^{-1} for 30
178 seconds and 1.3×10^{-6} s^{-1} for 300 seconds, thus yielding an average of 6.5×10^{-6} s^{-1}. This
179 cyclicity was applied in an attempt to best simulate the cyclic pressurisation inferred from
180 volcanic conduits (Vinciguerra et al., 2005). Based on the magma viscosity determination and
181 the rock mechanical tests, the experiments were performed at temperatures of 828 °C, 892 °C
182 and 918 °C in order to observe the potential influence of the magma on the host rock. During
183 the experiments, the force applied to the melt was transmitted as an internal fluid (magma)
184 pressure (due to the incompressibility of the silicate melt) onto the conduit inner shell (e.g.
185 Valko and Economides, 1995). Essentially, the magma pressure acts against the inner surface
186 of the conduit inducing failure in a manner analogous to hydrofracturing in rock mechanics.
187 Deformation and failure was additionally monitored by a pair of acoustic emission (AE)
188 sensors mounted directly on the loading pistons, to record the microseismicity generated at
189 the point of shell failure; this microseismicity was scaled to fracturing on the tectonic scale
190 (Burlini et al., 2007; Benson et al., 2007, 2010). The experiments were halted after failure of
191 the shell, as confirmed by an obvious peak in AE energy and a substantial (to near-zero value)
192 axial stress drop. The samples were then subjected to structural analysis, and the mechanical
193 data were used in a numerical computation.
194

195 Post-experimental structural analyses were performed on the sample using neutron
196 computed tomography (NCT), carried out at the ANTARES detector and FRM II cold
197 neutron beam facility installed at Garching, Germany (Muhlbauer et al., 2005). Reconstructed
198 images from the NCT have a voxel size of approximately 40 μm, permitting a simplified 3-D

199 reconstruction of the internal structure of the samples and the extensive fracture patterns
200 produced by the tensile stresses. Moreover, examination of the fracture network was also
201 performed using transmitted light and reflected fluorescent light microscopy.
202
203
204 **3. Results and analysis**
205
206 *(i) Conduit melt viscosity*
207
208 The temperature dependence of viscosity investigated through micropenetration
209 shows that the Cougar Creek rhyolitic melt is a strong melt (low fragility index), with a near
210 Arrhenian behaviour (Fig. 2). The viscosity data shows a standard deviation below 0.05 log
211 unit of viscosity. Application of the Vogel-Fulcher-Tammann (VFT) equation resolves the
212 viscosity (η) to:
213
214 (2)
215
216 where T is the temperature in Celsius, valid between the investigated temperature range of
217 750 and 920 °C, and A = -0.6505, B = 7342, and C = -132.
218
219
220 *(ii) Uniaxial compressive strength of the basalt*
221
222 The uniaxial compressive strength of the basalt was investigated at a range of
223 temperatures (25, 200, 500, 750, 900 and 950 °C) in order to probe potential changes in the
224 mechanical behaviour. Brittle failure was observed in all samples (Fig. 3). Below 950 °C the
225 strength remained approximately 150 MPa and did not vary systematically with temperature.

226 At 950 °C the sample demonstrated mild changes in the mechanical behaviour, resulting in an
227 increase in the peak stress and total strain at failure. Altogether, the data yielded values
228 comparable to complementary studies (e.g., Heap et al., 2010).
229
230
231 *(iii) Magma-rock failure test*
232
233 The mechanical behaviour of conduit failure due to magma pressurisation was
234 investigated at three temperatures. Figure 4 shows the evolution of stress (axially generated
235 on the cylindrical end of the inner melt core) with strain of the magma. During the experiment
236 at 828 °C (Fig. 4A), the first detection of accumulated stress occurred at approximately 2570
237 s, with a subsequent stress drop noted as the strain rate entered its deceleration phase. The
238 next cycle of strain rate acceleration/deceleration was also accompanied by a stress
239 concentration/drop. The character of the third, fourth and fifth cycles of strain rate
240 acceleration/deceleration were, however, significantly different in that a much higher stress
241 accumulation was measured, of 25, 38 and 45 MPa respectively, and in each case an
242 exponential stress drop occurred that did not fully recover to zero before the onset of the
243 subsequent strain acceleration. The onset of pressure accumulation further coincided with the
244 continuous release in acoustic emissions. The fifth and final cycle induced a stress drop to a
245 low value (6-7 MPa) as a result of the complete failure of the outer shell. Failure was
246 accompanied by a momentary increase in acoustic emissions. The two subsequent cycles of
247 strain rate acceleration/deceleration showed that stress was incapable of accumulating and
248 that acoustic emissions were fluctuating. The data show a clear dependence of the conduit
249 pressure on the strain rate, since the peak stress increases in subsequent cycles, and the stress
250 is released during the strain deceleration phases.
251
252 The general observations of stress concentration and relaxation as well as the
253 accompanying acoustic emissions remain similar for all magma-conduit pressurisation tests,

254 irrespective of the temperature. Temperature, which according to our investigation lowers the
255 melt viscosity more than it affects the elastic behaviour of the shell (Fig. 2 vs. 3), speeds up
256 relaxation during strain rate deceleration and delays failure of the shell (Fig. 4B, Fig. 4C). As
257 the temperature increases the number of acceleration/deceleration cycles that lead to a lasting
258 concentration of stress increases; once the stress accumulates, it is easier to maintain over
259 time during the periods of slower strain rate (e.g. Fig. 4B 1050s & 10500s compared to Fig.
260 4C 10250s & 10700s).
261
262
263 **4. Analysis**
264
265 *(i) Structural analysis*
266
267 Optical observation of the samples after the experiments clearly illustrates the tensile
268 nature of the cracks that developed (Fig. 5). In plan view, the samples display two or three
269 tensile cracks separated by angles of 180 or 120 degrees, respectively, which illustrate the
270 axisymmetric nature of the setup. Axially, these cracks extend the entire length of each shell.
271 The aperture of each fracture varies between each experiment; in some cases (Fig. 5, YE3),
272 the sample fractured violently resulting in the presence of large glass fragments in the tensile
273 cracks (Lavallée et al., 2011).
274
275 Post-test neutron computed tomography images of the sample revealed the continuity
276 of each tensile fracture developed, from the outer to the inner margin of the shell (Fig. 6). An
277 in-depth examination of the cracks clearly shows that they extend further into the rhyolite
278 conduit. Microscopic analysis provides further details of the geometry of the cracks in the
279 glass, which was a melt as it underwent brittle deformation. In detail, we observe a
280 fragmented area hosting multiple micrometric cracks, converging towards the rupture tips,
281 some 600 microns inside the glass (melt). The ability of a melt to fracture requires a strain

rate faster than its relaxation rate. A complementary analysis of the criterion for failure of the melt during conduit fracturing is presented in Lavallée et al. (2011), suggesting that at the high strain rates inherent in these processes, even low-viscosity melts will deform in a brittle manner (e.g., Dingwell and Webb, 1989).

(ii) Visco-elastic relaxation

The stress-time data was analysed by considering (1) the relaxation of the stress during each period of strain rate deceleration, and (2) the peak stress at failure as a function of temperature (see *section iii* below). These respectively provided information on the rheological contribution of the melt and the mechanical contribution of the rock.

By examining the time-scale of stress release, it is possible to extract a quantitative relationship between the dynamic modulus of the melt in the conduit and the stress decay rate prior to shell failure. The analysis makes use of the known viscosity of the central rhyolitic melt at the temperatures of interest (Fig. 2), in order to derive an apparent modulus for the melt. Four cycles of strain-hold are considered prior to shell failure, and the Maxwell model adapted by Richter (2006) is used. This application is possible because the viscosity of a Newtonian melt remains constant at the tested strain rates:

(3)

This analysis delivers the Young's modulus of the inner conduit (melt); however, for the purposes of our study, we adopt a generalized 'apparent' modulus (M_a). Other variables include time t, loading time t_L, peak stress σ_0, stress at time σ_t, and tensile viscosity η_t (Eqn. 3). Figure 7 illustrates the first 100 s immediately after the commencement of the deceleration

segments of the four cycles preceding shell failure (for each of the three experiments shown in Fig. 3). Application of Eqn. 3 using measured viscosities of 8.3, 9.6 and 10 log unit (in Pa*s), thus permits the calculation of the conduit stiffness with each cycle and temperature (Fig. 8). For all experiments, the stress decay exponent decreases (i.e. becomes flatter) moving from cycle 1 to 4. In terms of material stiffness, this result shows a decrease in modulus M_a from 180 to 30 MPa at 828 °C, from 80 MPa to 10 MPa at 892 °C and from 8 MPa to nearly zero MPa in the case of 918 °C. This suggests that the apparent modulus decreases as stress accumulates on the outer shell, leading to failure, as the temperature increases.

(ii) Peak stress at failure

The outer shell is most likely to fail when the hoop stress at its boundary exceeds the limiting tensile strength of the basalt. It is possible to estimate the tensile strength of the basalt shell using a combination of setup geometry and knowledge of the Young's modulus, the Poisson's ratio, and the material stiffness (as provided by Rocchi et al., 2004; Heap et al., 2011; Selvadurai and Benson, 2012). This analysis provides a direct measure of the stress accumulated in the magma at failure, and thus the resistance of magma to dyking.

In a recent study, Selvadurai and Benson (2012) theoretically examined the problem of the internal pressurisation of a hollow elastic cylinder of internal radius a and external radius b by a smoothly embedded cylindrical elastic inclusion of identical length. The objective of their study was to use the smoothly embedded cylindrical elastic inclusion as a device for exerting a radial stress at the interface, which in turn would induce a tensile stress field in the hollow elastic cylinder. The use of an elastic cylindrical inclusion or plug to induce the hoop stress state in the annular cylinder is considered to be a more convenient and

336 controllable loading configuration as opposed to the application of fluid pressures, which
337 would entail abrupt rupture of the outer cylinder, particularly if the aspect ratio $(b/a)=\Gamma$ is
338 marginally in excess of unity. The provision of a smooth interface between the cylindrical
339 inclusion and the annular cylinder lends itself to the development of a relatively convenient
340 closed form analytical solution based on the classical theory of elasticity. In an experiment,
341 this interface has to be smooth to ensure the applicability of the theoretical results. [Note: The
342 alternative to account for axial friction between the inner core and the external annular
343 cylinder is much more difficult and the stress analysis of the resulting problem can only be
344 performed through a computational approach (Selvadurai and Boulon, 1995).]
345
346 In the context of the application of the theoretical derivation to the present magma
347 pressurisation problem, the outer annular cylinder can be regarded as the basaltic shell with
348 isotropic Young's modulus E_R and Poisson's ratio ν_R and the inner closely fitting elastic
349 inclusion can be regarded as the conduit core of rhyolitic melt of isotropic Young's modulus
350 E_C and Poisson's ratio ν_C. The inner core is subjected to a uniform axial compressive stress σ_A
351 and the outer boundary of the annular basalt cylinder is maintained traction free. The analysis
352 of the resulting elasticity problem is straightforward and the assumption of complete contact
353 at the interface between the inner core and the external cylinder ensures that the radial
354 displacement and the radial tractions exhibit continuity (Timoshenko and Goodier, 1970;
355 Davis and Selvadurai, 1996; Selvadurai, 2000). The specifics of the analysis of the elastic
356 plug compression problem are given in Selvadurai and Benson (2012), who also use the
357 elastic inclusion compression approach to estimate the tensile strength of annular cylinders of
358 Stanstead Granite. These studies also present an approach for estimating the Mode I fracture
359 toughness of the geomaterial. The result of primary interest to the present paper relates to the
360 tensile hoop stress that is generated at the boundary of the annular rock cylinder during
361 compression of the central cylindrical elastic core by the axial compressive stress σ_A, which

can be evaluated in exact closed form. For example, the tensile hoop stress at the inner boundary of the outer cylindrical rock can be evaluated using:

(4)

It is clear that in order for these stresses to develop, $\nu_C \neq 0$ and the analysis (Selvadurai and Benson, 2012) shows that the interface compressive stress is identical to the tensile hoop stress generated at the boundary of the rock. Of specific interest are the results applicable to the limiting case where the outer boundary of the core extends to infinity (i.e. $\Gamma \to \infty$). In this case the above results yield:

(5)

Known parameters in Eqns (4) and (5) include the applied stress σ_A, the ratio of conduit to shell diameter Γ, the Poisson's ratios and Young's moduli for the outer shell and the core (ν_C , E_C) and (ν_R , E_R) respectively. The modulus of the conduit is calculated from the stress relaxation stage of the experiment discussed previously, leaving only the Poisson's ratio of the melt (0.35 ± 0.05) that is taken from previously published model data (Lister and Kerr, 1991). This permits the tensile stress to be calculated as a function of the applied stress. If this stress at the boundary of the country rock reaches the limiting tensile strength, fracture will occur.

384 To compare the theoretical fracture criteria with the laboratory data, Figure 9 shows the
385 theoretical (hoop) stress (given by Eqn. (4)) as a function of the applied stress and a 'family'
386 of representative Poisson's ratios (0.3-0.35-0.4) for the conduit, superimposed with the actual
387 stress at which the samples failed (arrows). A clear relationship is seen whereby higher
388 temperatures require a lower conduit pressure in order to produce the same hoop stress,
389 leading to fracture of the outer shell.
390
391
392 **5. Discussion and conclusions**
393
394 The dynamics of fracturing and associated magma movement through dykes is central to
395 our understanding of mass transport and ultimately to our descriptions of volcanic eruptions
396 (McNutt, 1996; Carracedo, 1999; Gudmundsson and Brenner, 2004; Collinson and Neuberg,
397 2011). Indeed, the accuracy of forecasting volcanic hazards posed by the propagation of
398 dykes, as well as the stability/integrity of a volcanic conduit, strongly relies on probing the
399 state of the host rocks at depth (e.g. Nakamura, 1977; Gudmundsson and Loetveit, 2005) – a
400 task that cannot be achieved with current state of knowledge regarding monitored geophysical
401 signals alone (McNutt, 1996; Smith et al., 2009). Models require the input of the path leading
402 to various conduit fracture properties at depth and in volcanic edifices (e.g. Gudmundsson and
403 Brenner, 2001; Vinciguerra et al., 2004). The present experimental and analytical
404 investigation of magma-rock coupling to the problem of dyke initiation demonstrates the
405 strong relationship between magma rheology and host rock elasticity. A decrease in the
406 apparent Young's modulus of the magma precedes the tensile fracture of the host rock, which
407 generates a local strain rate capable of fragmenting the magma.
408
409 Material stiffness is a key parameter of volcanic melts, and in many cases it is intimately
410 linked to the explosivity of magma (e.g. Dingwell, 1996). The ability to estimate an apparent
411 modulus of magma at depth would be helpful; since direct measurements are impractical,

412 complimentary means must be employed to obtain such data. Our analysis suggests that it is
413 possible to do so by incorporating measured viscous and elastic parameters (e.g. Table 1) in
414 Eqn (4). For the case of the competent outer basalt shell, the Young's modulus and Poisson's
415 ratio were measured directly and found to be essentially temperature invariant within our
416 investigated temperature range (Heap et al., 2009), which is in broad agreement with the work
417 of Rocchi et al., (2004). Likewise, the viscosity of the rhyolite melt is also known as a
418 function of temperature. The least constrained parameter, the Poisson's ratio of the melt, was
419 given a central value of 0.35 with a spread of 0.05 to calculate the tensile fracturing. The
420 lower and centre estimates for Poisson's ratio within this range have been suggested in the
421 small number of studies done to date (Gudmundsson, 1988; Rubin, 1995; Carpenter and Cash,
422 1988; Chu et al., 2010), with the upper end data measured at room temperature. Our analysis
423 resolves the tensile (hoop) stress required to fracture the outer shell to be approximately 7 to
424 11 MPa, irrespective of the viscosity of the conduit. This agrees with field estimates for the
425 tensile strength of rocks important in dyke propagation of approximately 6 to 9 MPa
426 (Gudmundsson, 2011a; 2011b).
427
428 The stress relaxation is analysed using the Maxwell-Zener model (Richter, 2006).
429 Specifically, our experiments suggest that a noticeable decrease in the apparent modulus M_a
430 precedes failure. Although this is counterintuitive, such an effect could be produced if, as the
431 cycles proceeded, an increase in shear stresses is present on the boundary of both the conduit
432 and the inner shell surface. This is definitely a possibility since, in our experiment,
433 pressurisation of the magma against the conduit wall is accompanied by an increased surface
434 area of contact (i.e., initially, there is a narrow <0.1mm gap between the melt and the shell
435 due to abrasion during sample preparation). Additionally, there may be rheological changes
436 taking place due to melt pressurisation. Whether thixotropy of the melt comes into play in our
437 investigation is rather unlikely since pressurisation of the low-viscosity melt was performed at
438 strain rates far slower than the onset of non-Newtonain behaviour calculated via Maxwell
439 relaxation time scale (e.g., Dingwell and Webb, 1989; see Lavallée et al., 2011). As to the

likelihood that the visco-elastic behaviour of the melt is modified with increasing pressurisation, magmas are generally regarded as visco-elastic liquids with very restricted influence of pressure on the viscosity (Dingwell, 1998). It thus seems most likely that the observed apparent modulus decrease results from a combination of viscous relaxation and release of the elastic stress of the shell accumulated at the inner margin. The ability to probe for this apparent modulus in nature would thus offer a window for both the magma viscosity and the conduit wall elastic response.

Finally, it should be emphasized that the post-failure observations revealed fracturing of the melt inside the conduit. Rheological and acoustic analysis of the criterion for failure of the melt during conduit fracturing is presented in Lavallée et al. (2011), suggesting that at the high strain rates inherent in these processes, even low-viscosity melts will deform in a brittle manner (e.g., Dingwell and Webb, 1989). A close analysis of the fracture tip and surrounding crack geometry reveals a remarkable similarity to a Mach cone. Such 'shock cone' features generally form in spontaneously nucleated supershear ruptures, propagating faster than the local speed of sound (e.g. Xia et al., 2004), fossilized here in the (formerly molten) rhyolite at an angle θ to the fracture. Whether the cone formed as a result of sub-Rayleigh tensional cracking of the melt during conduit shell failure or due to spontaneous supershear rupture cannot be ascertained through our post-experiment analysis; it nonetheless remains evident that magma can fragment during wall rock failure. This observation alone is important to our understanding of dyke nucleation and propagation, because not only does magma failure instigate the generation of tuffisite veins (Lavallée et al., 2011), it also contributes to the seismic record (Lavallée et al., 2008; Tuffen et al., 2003, 2008), masking the precursor signal for dyke propagation and, potentially, explosive eruptions.

In summary, the combined experimental (mechanical and AE) and analytical simulations of conduit failure induced by the inner compression of magma show that:

(a) The coupling of stress, strain and seismic data through time can be used to infer the stability of volcanic conduits and/or the state of the magma during periods of unrest via the calculation of viscoelastic relaxation parameters and hence the modulus (or viscosity) of the melt.

(b) Dyke nucleation initiates when the tensile strength of the host rocks is overcome by the magmatic pressure. In the case of the investigated basalt from Mt. Etna, the calculated tensile strength is temperature invariant and approximates 7 to 11 MPa.

(c) Conduit wall rock failure generates an energetic strain wave, with some evidence of this being a supershear feature, capable of locally fragmenting magma, thereby promoting the production of tuffisite veins and, potentially, episodes of explosive activity.

Acknowledgements

P. Benson thanks S. Vinciguerra for sample collection assistance (Etna) and Benoit Cordonnier for many fruitful discussions. Y. Lavallée acknowledges funding from the Deutschforschungsgemeinschaft (DFG) project LA2651/1-1. M. Heap was funded by MatWerk. A. Flaws and K.-U. Hess were funded from the DFG project HE4565/2-1. D.B. Dingwell acknowledges an LMUexcellent Research Professorship in Experimental Volcanology of the Bundesexzellenzinitiative, the DFG projects DI 431/35-1 and 35-2. The development of neutron tomographic tools employed here was supported by the Schwerpunktprogramm of the DFG. M. J. Heap and D. B. Dingwell also acknowledge the support of a Hubert Curien Partnership (PHC) PROCOPE grant (grant number 27061UE), the Deutscher Akademischer Austauschdienst (DAAD) in Germany, and the Ministry of Foreign and European Affairs (MAE) and the Ministry of Higher Education and Research (MESR), both in France. The authors thank Sally Selvadurai for editorial (copyedit) assistance, and August Gudmundsson and one anonymous reviewer whose comments greatly improved the manuscript.

References

Acocella, V., F. Cifelli, and R. Funiciello (2001), The control of overburden thickness on resurgent domes: insights from analogue models, *J. Volc. Geotherm. Res.*, 111, 137-153.

Balme, M. R., V. Rocchi, C. Jones, P.R. Sammonds, P.G. Meredith, and S. Boon (2004), Fracture toughness measurements on igneous rocks using a high-pressure, high-temperature rock fracture mechanics cell, *J. Volc. Geotherm. Res.*, 132(2-3), 159-172.

Benson, P. M., B. D. Thompson, P. G. Meredith, S. Vinciguerra, and R. P. Young (2007), Imaging slow failure in triaxially deformed Etna basalt using 3D acoustic-emission location and X-ray computed tomography, *Geophys. Res. Lett.*, 34, L03303, doi:10.1029/2006GL028721.

Benson, P.M., S. Vinciguerra, P.G. Meredith, and R.P. Young (2010), Spatio-temporal evolution of volcano seismicity: A laboratory study, *Earth Planet. Sci. Lett.*, 297, 315–323

Bonafede M. and S. Danesi (2010), Near-field modifications of stress induced by dyke injection at shallow depth, *Geophys. J. Int.*, 130, 435-448, DOI: 10.1111/j.1365-246X.1997.tb05659.x

Broek, D. (1982), Elementary Engineering Fracture mechanics, Martins Nijhoft Publishers, the Hague, Netherlands.

Burlini, L., S. Vinciguerra, G. Di Toro, G. De Natale, P.G. Meredith, and J.-P. Burg (2007), Seismicity preceding volcanic eruptions: new experimental insights, Geology, 35, 183-186.

Carracedo, J. C. (1999), Growth, structure, instability and collapse of Canarian volcanoes and

comparisons with Hawaiian volcanoes, *J. Volc. Geotherm. Res.*, 94, 1 – 19.

Carrigan, C.R. (2000), Plumbing systems. In: Sigurdson, H. (Ed.), Encyclopedia of Volcanoes. Academic Press, London, pp. 219–235.

Carpenter, P.J., and D.J. Cash (1988), Poisson's ratio in the valles caldera and Rio Grande rift of Nothern New Mexico, *BSSA*, 78(5), 1826-1829

Chen, Z. and Z.-H. Jin (2011), Subcritical dyke propagation in a host rock with temperature-dependent viscoelastic properties, *Geophys. J. Int.,* doi: 10.1111/j.1365-246X.2011.05113.x

Christiansen, R. L. (2001), The Quaternary and Pliocene Yellowstone plateau Volcanic Field of Wyoming, Idaho and Montana, U.S. Department of the Interior, U.S. Geological Survey, Professional Paper 729–G, U.S. Geological Survey, Reston, Virginia.

Chu, R., D. V. Helmberger, D. Sun, J. M. Jackson, and L. Zhu (2010), Mushy magma beneath Yellowstone, *Geophys. Res. Lett.*, 37, L01306, doi:10.1029/2009GL041656.

Collinson, A.S.D. and J.W. Neuberg (2011), Permeability Controls on Gas Storage and Transport in a Permeable Volcanic Edifice. Submitted to *J. Volc Geotherm. Res.*

Cuevas J., J.J. Esteban, and J.M. Tubia (2006), Tectonic implications of the granite dyke swarm in the Ronda peridotites (Betic Cordilleras, Southern Spain), *J. Geol. Soc.* 163, 631-640, DOI: 10.1144/0016-764905-038

Davis, R.O. and A.P.S. Selvadurai (1996), Elasticity and Geomechanics, Cambridge University Press, Cambridge.

De Natale, G., S.M. Petrazzuoli, and F. Pingue (1997), The effect of collapse structures on ground deformations in calderas, *Geophys. Res. Lett.*, 24(13), 1555–1558.

Dingwell, D.B. and S.L. Webb (1989), Structural relaxation in silicate melts and non-Newtonian melt rheology in geologic processes, *Phys. Chem. Miner.*, 16 (5), 508–516.

Dingwell, D. B. (1996), Volcanic dilemma: Flow or blow?, *Science*, 273(5278), 1054-1055.

Dingwell, D.B. (1998), Melt viscosity and diffusion under elevated pressures, *Rev. Min. Geochem.*, 37, 397-424.

Griffith, A. (1920), The phenomena of rupture and flow in solids, *Philos. Trans. Roy. Soc. London*, Series A, 221, 163-198.

Gudmundsson, A. (1988), Effect of tensile stress concentration around magma chambers on intrusion and extrusion frequencies, *J. Volc. Geotherm. Res.*, 35, 179-194

Gudmundsson, A. (2009), Toughness and failure of volcanic edifices, *Tectonophysics*, 471(1-2), 27-35.

Gundmundsson, A. (2011a), Deflection of dykes into sills at discontinuities and magma-chamber formation, *Tectonophysics,* 500, 50–64.

Gudmundsson, A. (2011b), Rock Fractures in Geological Processes, 592pp, CUP.

Gudmundsson, A. and S.L. Brenner (2001), How hydrofractures become arrested, *Terra Nova*, 13(6), 456-462.

Gudmundsson, A. and S.L. Brenner (2004), Local stresses, dyke arrest and surface deformation in volcanic edifices and rift zones, *Ann. Geophys.*, 47(4), 1433-1454.

Gudmundsson, A. and I.F. Loetveit (2005), Dyke emplacement in a layered and faulted rift zone, *J. Volc. Geotherm. Res.*, 144, 311–327.

Heap, M. J., Vinciguerra, S. and Meredith, P. G., 2009. The evolution of elastic moduli with increasing crack damage during cyclic stressing of a basalt from Mt. Etna volcano, *Tectonophysics*, 471, 153-160.

Heap, M. J., D. R. Faulkner, P. G. Meredith and S. Vinciguerra (2010), Elastic moduli evolution and accompanying stress changes with increasing crack damage during the cyclic stressing of rocks. *Geophysical Journal International*, 183, 225-236.

Heap, M. J., Baud, P., Meredith, P. G., Vinciguerra, S., Bell, A. F. and Main, I. G. (2011), Brittle creep in basalt: implications for time-dependent volcano deformation. *Earth and Planetary Science Letters,* 307, 71-82.

Hess, K.U. and D.B. Dingwell (1996), Viscosities of hydrous leucogranitic melts: A non-Arrhenian model. American Mineralogist, 81, 1297-1300.

Hess, K. U., B. Cordonnier, Y. Lavallée, and D. B. Dingwell (2007), High-load, high-temperature deformation apparatus for synthetic and natural silicate melts, *Review of Scientific Instruments*, 78(7), 075102.

Hutton, D.H.W. (1996), The ‘space problem’ in the emplacement of granite. *Episodes*, 19, 114-119.

Inglis, C.E. (1913), Stresses in a plate due to the presence of cracks and sharp corners, *Trans. Inst. Naval Architects*, 55, 219-241.

Jaeger, J., N.G.W. Cook and R. Zimmerman (2007), Fundamentals in Rock Mechanics (4th Edition), Blackwell Publishing, London. 475 pp.

Lavallée, Y., P.G. Meredith, D.B. Dingwell, K.U. Hess, J. Wassermann, B. Cordonnier, A. Gerik, and J.H. Kruhl (2008), Seismogenic lavas and explosive eruption forecasting, *Nature*, 453, 507–510.

Lavallée, Y., S. de Silva, G. Salas, and J.M. Byrnes (2009), Structural control of a rotated graben on volcanism at Ubinas, Huaynaputina and Ticsani, southern Peru. *J. Volcanol. Geotherm. Res.,* 186, 253-264.

Lavallée, Y., P. M. Benson, M. J. Heap, A. Flaws, K.-U. Hess, and D. B. Dingwell (2012), Volcanic conduit failure as a trigger to magmatic fragmentation, *Bull. Volc.,* 74, 11-13, doi: 10.1007/s00445-011-0544-2

Lejeune, A. M. and P. Richet (1995), Rheology of Crystal-Bearing Silicate Melts - an Experimental-Study at High Viscosities. *J. Geophy. Res.,* 100, 4215-4229.

Lister, J.R. and R.C. Kerr (1991), Fluid-mechanical models of crack propagation and their application to magma-transport in dykes, *J. Geophys. Res.*, 96, 10049-10077.

Massol, H. and C. Jaupart (1999), The generation of gas overpressure in volcanic eruptions. *Earth Planet. Sci. Lett.,* 166, 57– 70.

McNutt, S.R. (1996), Seismic monitoring and eruption forecasting of volcanoes; a review of the state-of-the-art and case histories, in Monitoring and mitigation of volcanic of volcanoes, edited by R. Scarpa and R. Tilling, pp. 99-146, Springer - Verlag, New York.

Menand, T., and S. R. Tait (2001), A phenomenological model for precursor volcanic eruptions, *Nature*, 411, 678-680.

Muhlbauer, M.J., E. Calzada, and B. Schillinger (2005), Development of a system for neutron radiography and tomography, Nuclear Instruments and Methods in Physics Research A, 542, 324–328

Nakamura, K. (1977), Volcanoes as possible indicators of tectonic stress orientation – principle and proposal, *J. Volc. Geotherm. Res.*, 2, 1-16.

Pertsov, N.V., B.S. Kogan, and V.N. Balashov (1977), Model of magma intrusions going through fractures under conditions of manifestation of effect of adsorption decrease of rock strength, *Doklady Akademii Nauk SSSR*, 235, 1375-1378.

Pitcher, W.S. (1979), The nature, ascent and emplacement of granitic magmas, *J. Geol. Soc. London*, 136, 627-662

Richter, F. (2006), Upsetting and Viscoelasticity of Vitreous SiO2: Experiments, Interpretation and Simulation. Technischen Universität Berlin, pp239.

Rocchi, V., P.R. Sammonds, and C.R.J. Kilburn (2004), Fracturing of Etnean and Vesuvian rocks at high temperatures and low pressures, *J. Volc. Geotherm. Res.*, 132, 137-157.

Rubin, A.M. (1995), Propagation of magma-filled cracks, *Ann. Rev. Earth Planet. Sci.*, 23, 287-336

Santoni, S., A. Tallarico, and M. Dragoni (2011), Magma ascent and effusion from a tensile fracture propagating to the Earth's surface, *Geophys. J. Int.,* 186, 681-698 . DOI: 10.1111/j.1365-246X.2011.05060.x

Selvadurai, A.P.S. (2000), Partial Differential Equations in Mechanics. Vol. II The Biharmonic Equation, Poisson's Equation, Springer-Verlag, Berlin.

Selvadurai, A.P.S. and Boulon, M.J. (Eds.) (1995), Mechanics of Geomaterial Interfaces, *Developments in Applied Mechanics*, Vol. 42, Elsevier Science Publ., Amsterdam.

Selvadurai, A. P. S. and P. M. Benson (2012), An elastic plug test for estimating properties of Brittle Geomaterials, *Int. J. Rock. Mech.* (In preparation).

Smith, R., P.R. Sammonds, and C.R.J. Kilburn (2009), Fracturing of volcanic systems: experimental insights into pre-eruptive conditions, *Earth Planet. Sci. Lett.*, 280, 211-219.

Sparks, R.S.J., M.I. Bursik, S.N. Carey, J.S. Gilbert, L.S Glaze, H. Sigurdsson, and A.W. Woods (1997), Volcanic Plumes. Wiley, New York.

Stanchits, S., S. Vinciguerra, and G. Dresen (2006), Ultrasonic velocities, acoustic emission characteristics and crack damage of basalt and granite, Pure Appl. Geophys., 163, 974 – 993.

Timoshenko, S.P. and Goodier, J.N. (1970), Theory of Elasticity, McGraw-Hill, New York

Tuffen, H., D.B. Dingwell, and H. Pinkerton (2003), Repeated fracture and healing of silicic magma generate flow banding and earthquakes? *Geology,* 31, 1089-1092.

Tuffen, H., R. Smith, and P.R. Sammonds (2008), Evidence for seismogenic fracture of silicic magma. *Nature,* 453, 511–514.

Valko and Economides (1995), Hydraulic fracture mechanics. Wiley. New York.

Vinciguerra, S., P. G. Meredith, and J. Hazzard (2004), Experimental and modelling study of fluid pressure-driven fractures in Darley Dale sandstone, *Geophys. Res. Lett.*, 31, L09609, doi:10.1029/2004GL019638.

Vinciguerra, S., D. Elsworth, and S. Malone (2005), The 1980 pressure response and flank failure of Mount St. Helens (USA) inferred from seismic scaling exponents, *J. Volc. Geotherm. Res.*, 144 (2005) 155– 168.

Walter, T.R. and V.R. Troll (2003), Experiments on rift zone evolution in unstable volcanic edifices, *J. Volc. Geotherm. Res.*, 127, 107-120.

Xia, K., A.R. Rosakis, and H. Kanamori (2004), Laboratory Earthquakes: The Sub-Rayleigh-to-supershear Rupture Transition, *Science*, 303, 1859-1861

Figure captions

Figure 1. Experimental setup in side view (left) and plan view (right). The composite sample of Cougar Creek Obsidian (CO) is encased by a shell of basalt (EB) and topped by a hard basaltic plug. Compression of the plug, and thus the rhyolitic melt, was achieved using a servo-controlled hydraulic apparatus, within a 3 zone split furnace (shown schematically by the red bars). Dimensions are in millimetres; note that the AE sensors are mounted some distance from the furnace to avoid damage.

Figure 2. Temperature dependence of the viscosity of Cougar Creek rhyolitic melt measured via the micropenetration technique in a Baehr vertical dilatometer.

Figure 3. Uniaxial compressive strength (UCS) of the basalt as a function of temperature. The UCS is largely independent of temperature up to 900 °C.

Figure 4. Mechanical data during the cyclic magmatic conduit pressurisation. The data combines the conduit stressing/relaxation (black), the axial strain accumulated in the magma (blue), and the monitored AE (red) as a function of time, for experiments at (A) 828 °C, (B) 892 °C and (C) 918 °C. Cyclicity in strain rate acceleration/deceleration can be clearly seen as pressurisation of the conduit at high strain rate, which is then followed by relaxation during the period of low strain rates. A surge of AE is observed when the outer jacket experiences tensile failure at approximately (A) 3550 s, (B) 10475 s, and (C) 10560 s.

Figure 5. Plan view images of the fractured outer shell, showing radial cracks in samples YE1 (828 °C), YE4 (892 °C), YE2 (918 °C) and YE3 (890 °C). The sketches below each image highlight the three (in the case of YE1), two (YE4 and YE2), or 4 (YE3) tensile cracks. At

high strain rates, samples occasionally fracture in a violent manner (sample YE3, 890 °C), see text for details. Sample diameter is 60 mm.

Figure 6. Sketch of the fractures along with neutron computed tomographic images and transmitted light microphotograph of sample YE2 at 918 °C (modified from Lavallée et al., 2011). Neutron computed tomographic images reveal the continuous nature of the radial cracks along the conduit length. Detailed microscopic examination further highlights the fracturing of the inner core of rhyolitic melt. In transmitted light, we observed converging cracks and propagation direction (arrows) akin to a 'Mach cone' fossilised in the melt due to the catastrophic failure of the outer shell. Such 'shock cone' features generally form when fractures propagate faster than the local speed of sound, preserved in the (formerly molten) rhyolite at an angle θ to the fracture. Such features have been simulated in other studies (e.g. Xia et al., 2004).

Figure 7. Stress relaxation segments (first 100 s only) for the last 4 cycles (as shown in Figure 4) prior to tensile failure of the confining basalt shell (Cycle 4 precedes failure).

Figure 8. Calculated apparent modulus (M) from viscoelastic relaxation parameters, using equation 3 (after Richter, 2006). The value of M is seen to decrease with both cycle number and increasing temperature.

Figure 9. Theoretical tensile failure strength as a function of internal magma pressure, inclusion modulus and temperatures. The magma pressurises until the shell fails in tension, denoted by arrows according to the maximum recorded conduit stress. Although the temperature of the experiments varies, a very similar hoop (tensile) stress at failure (i.e., 7 to 11 MPa) is calculated using Eqn. (6).

Figure 1.
Click here to download Figure: S.FIG1.eps

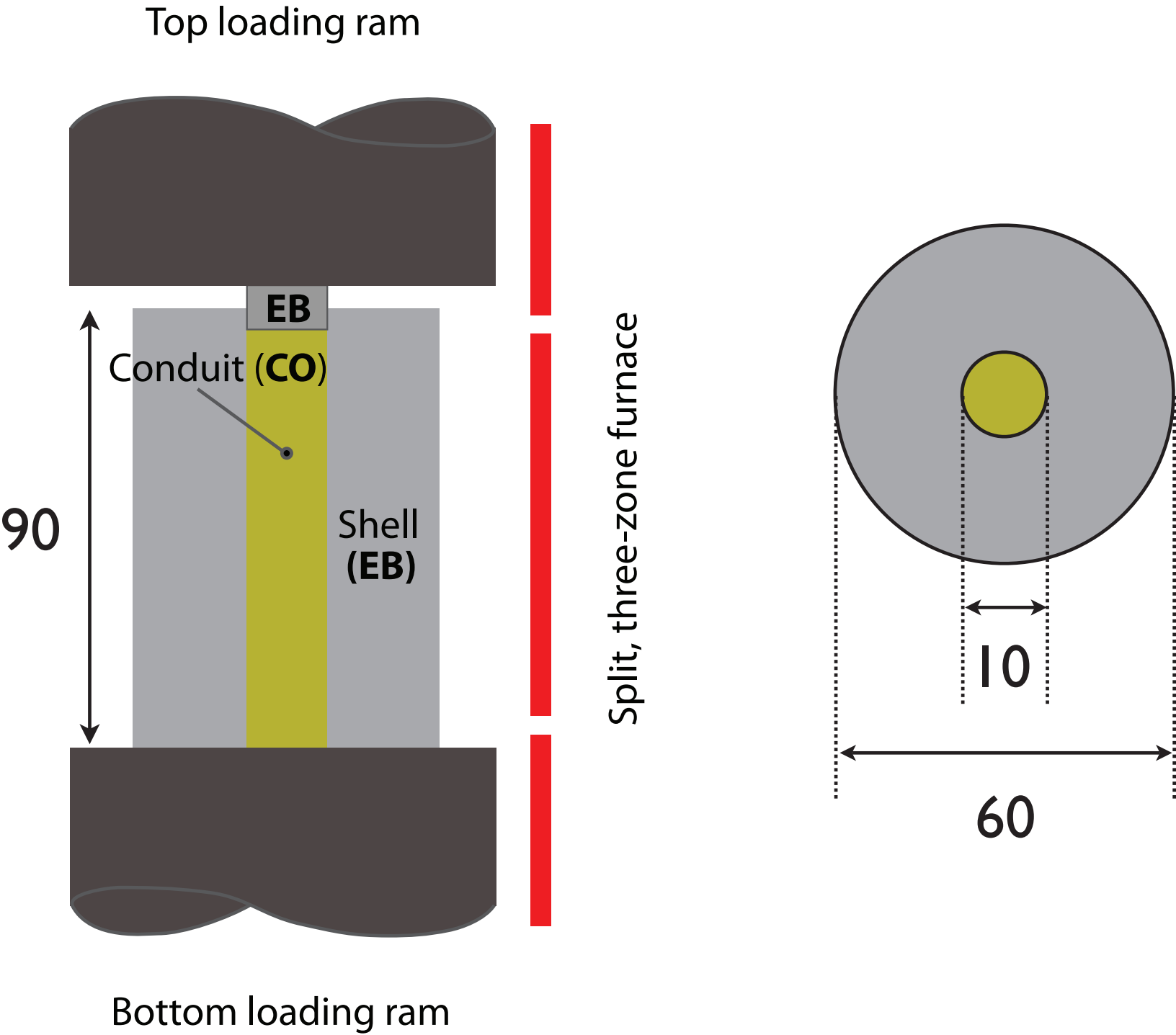

Figure 2.
Click here to download Figure: S_FIG2.eps

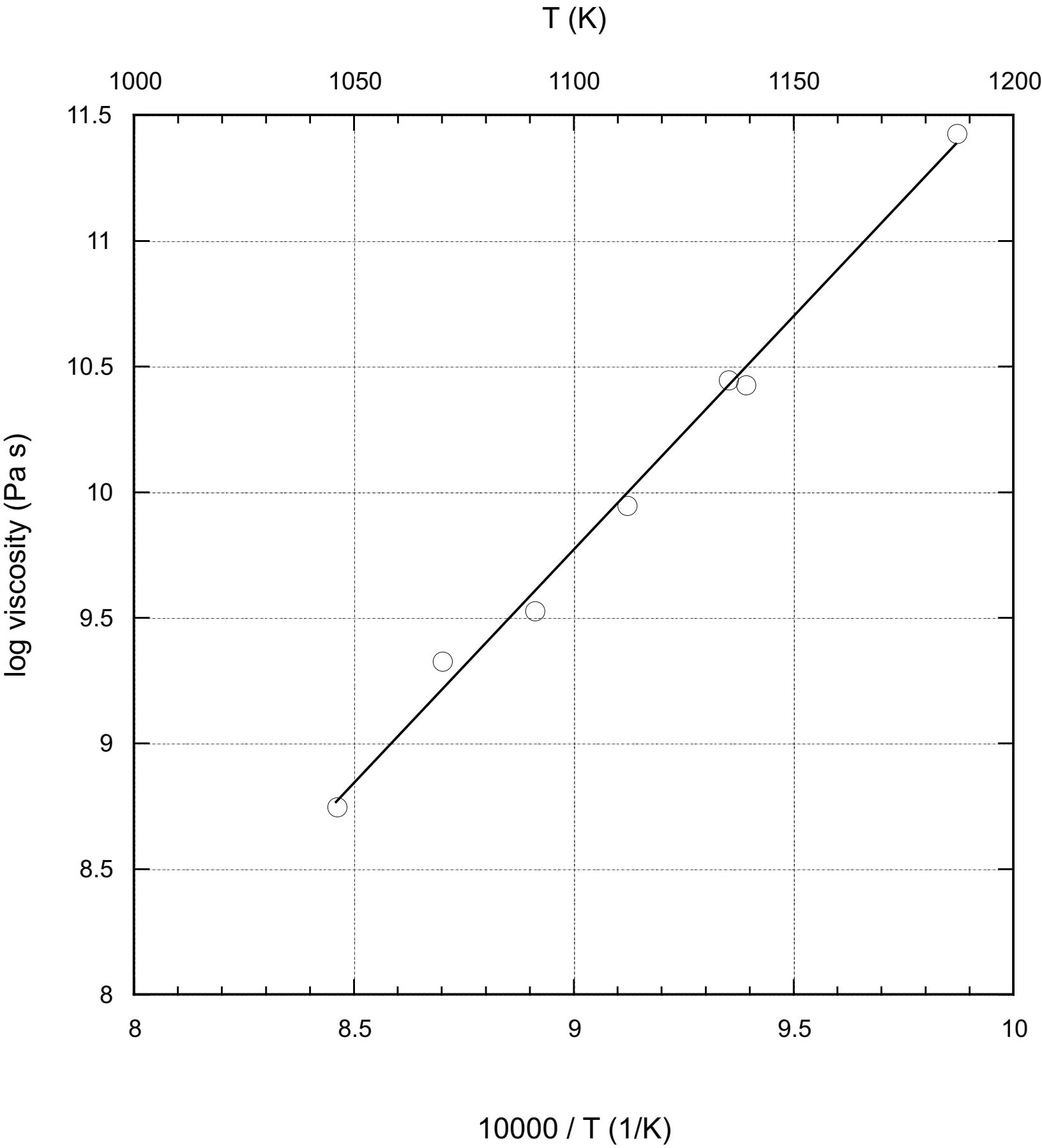

Figure 3.
Click here to download Figure: S_FIG3.eps

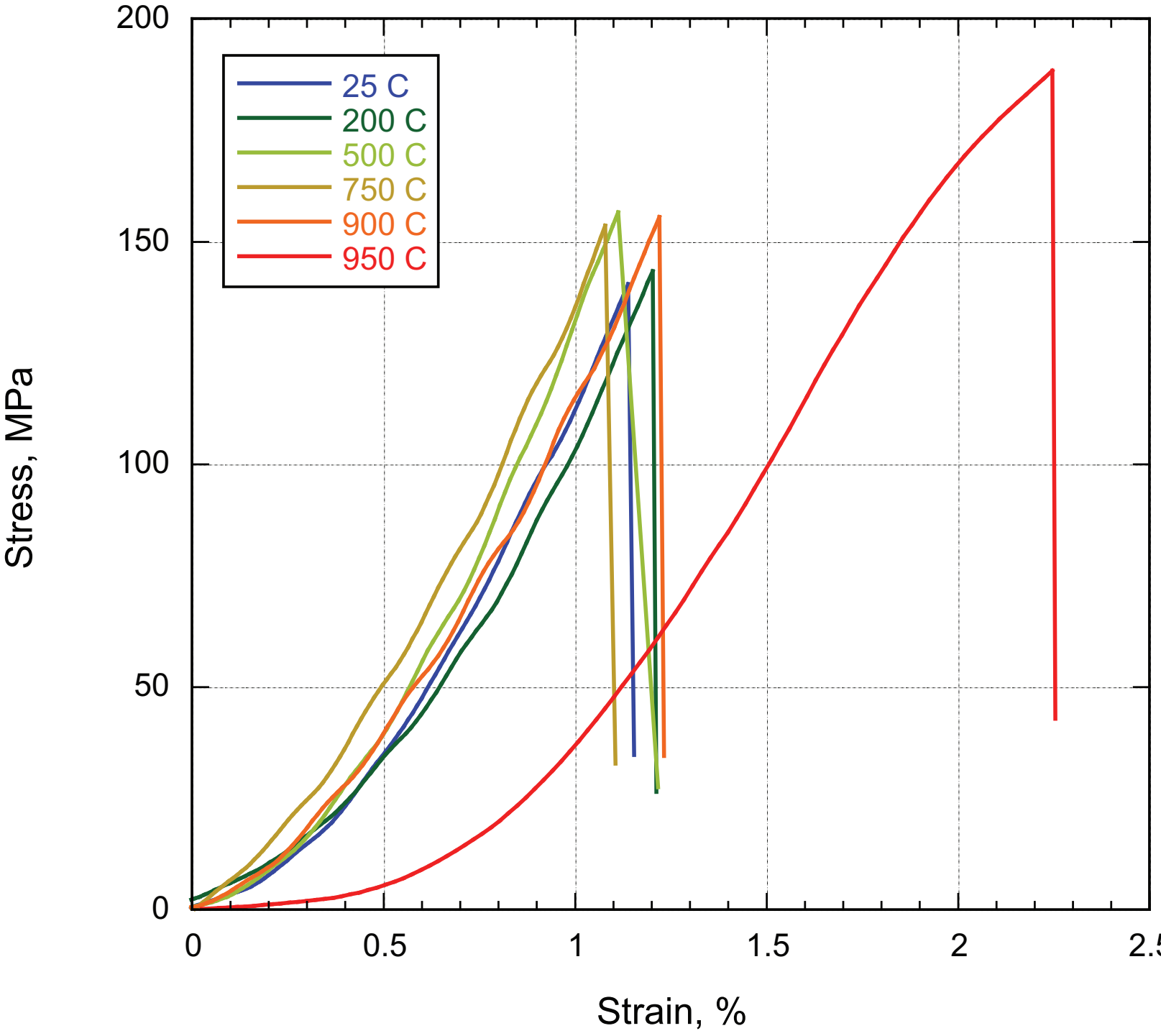

Figure 4.
Click here to download Figure: S_FIG4.eps

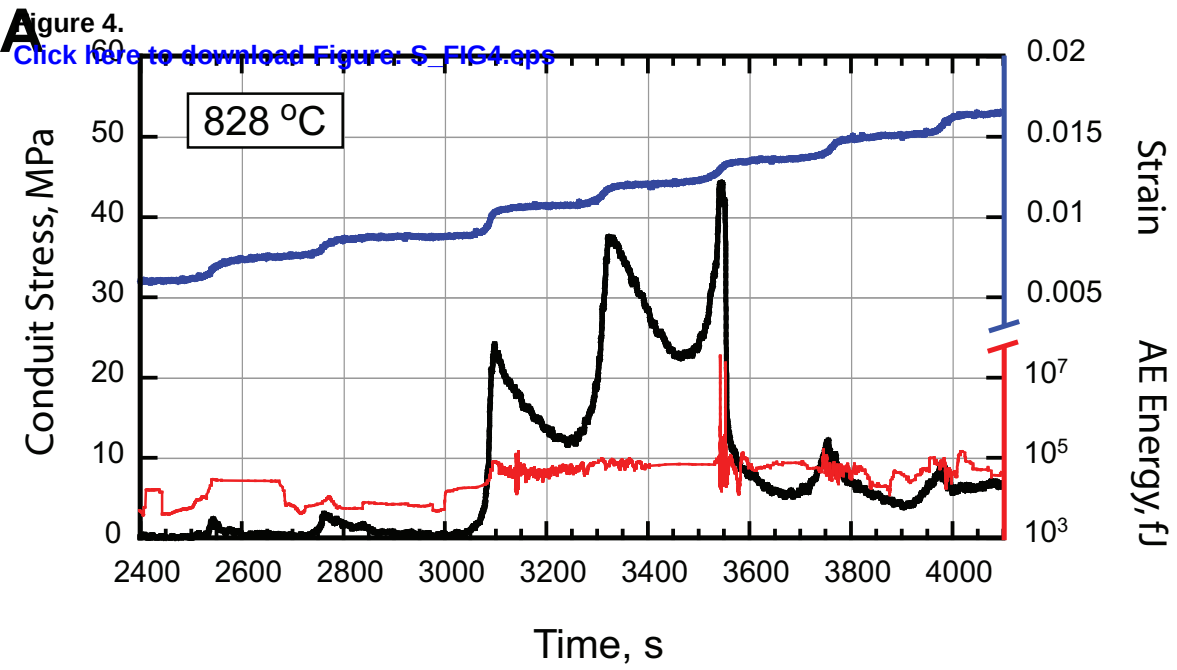

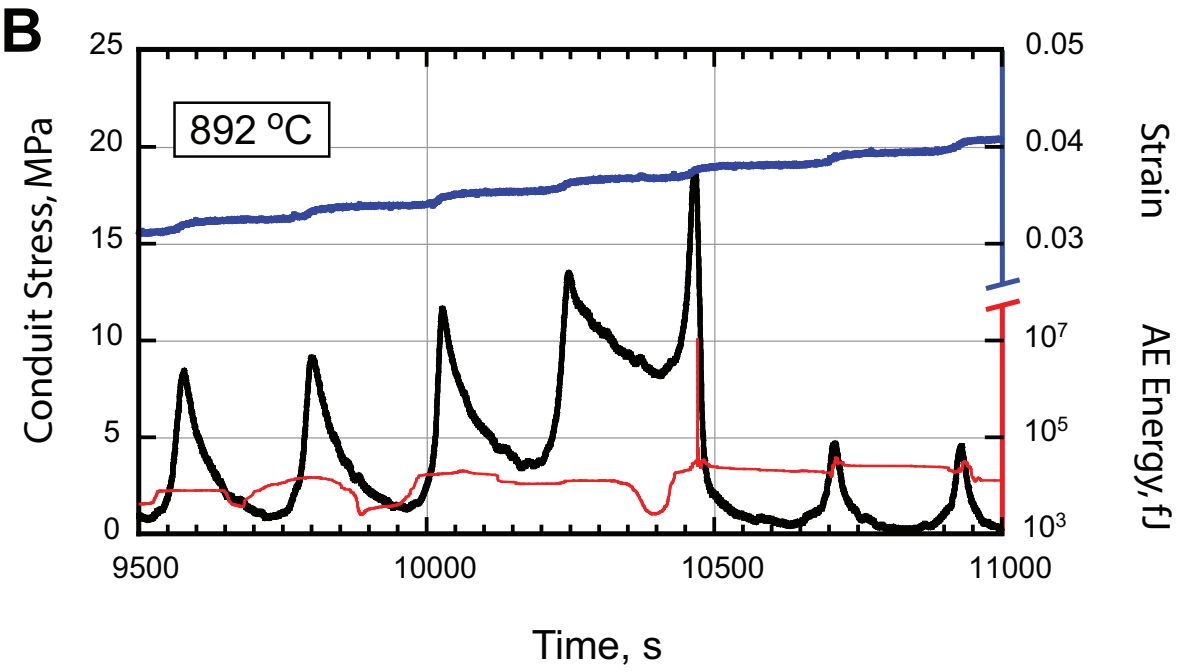

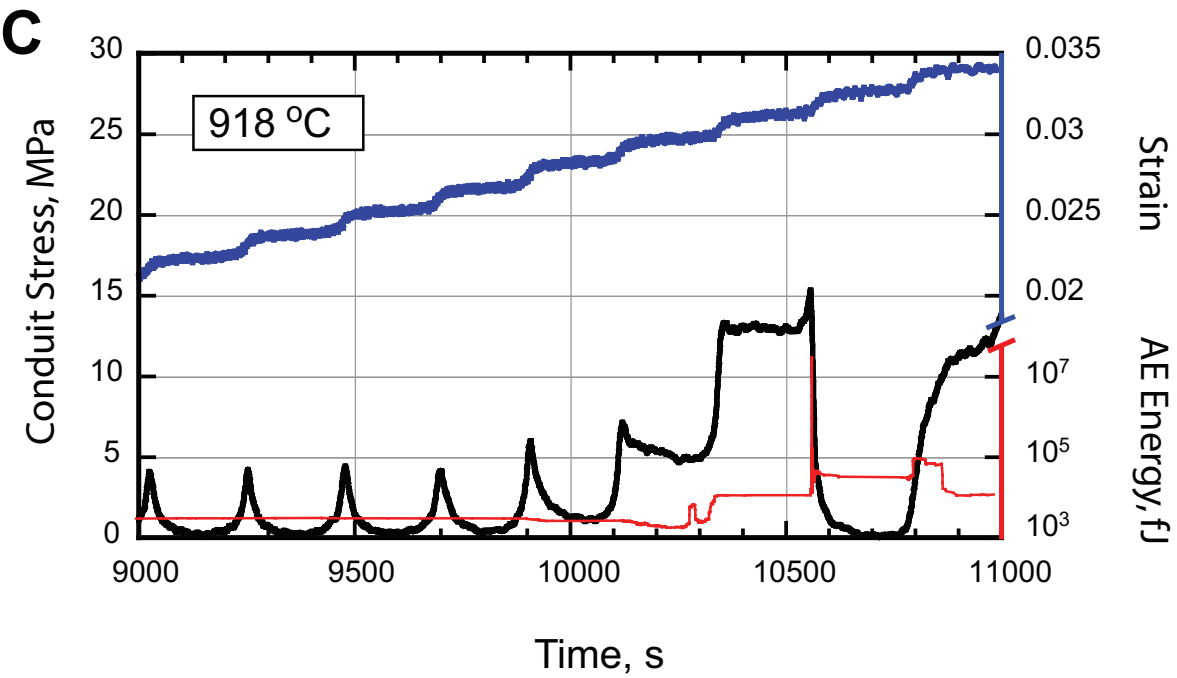

Figure 5.
Click here to download Figure: S_FIG5.eps

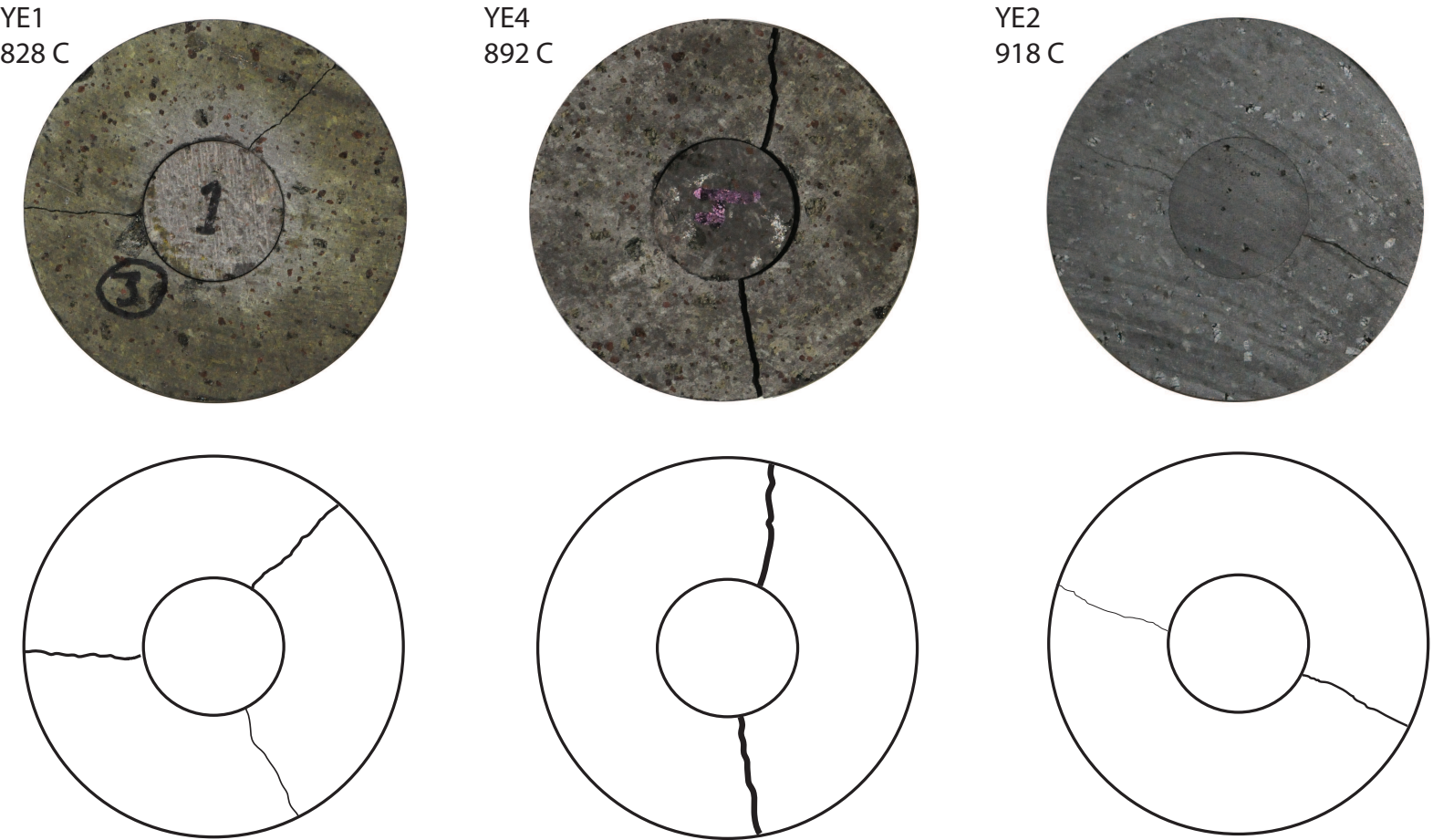

Figure 6.

Click here to download Figure: S_FIG6.eps

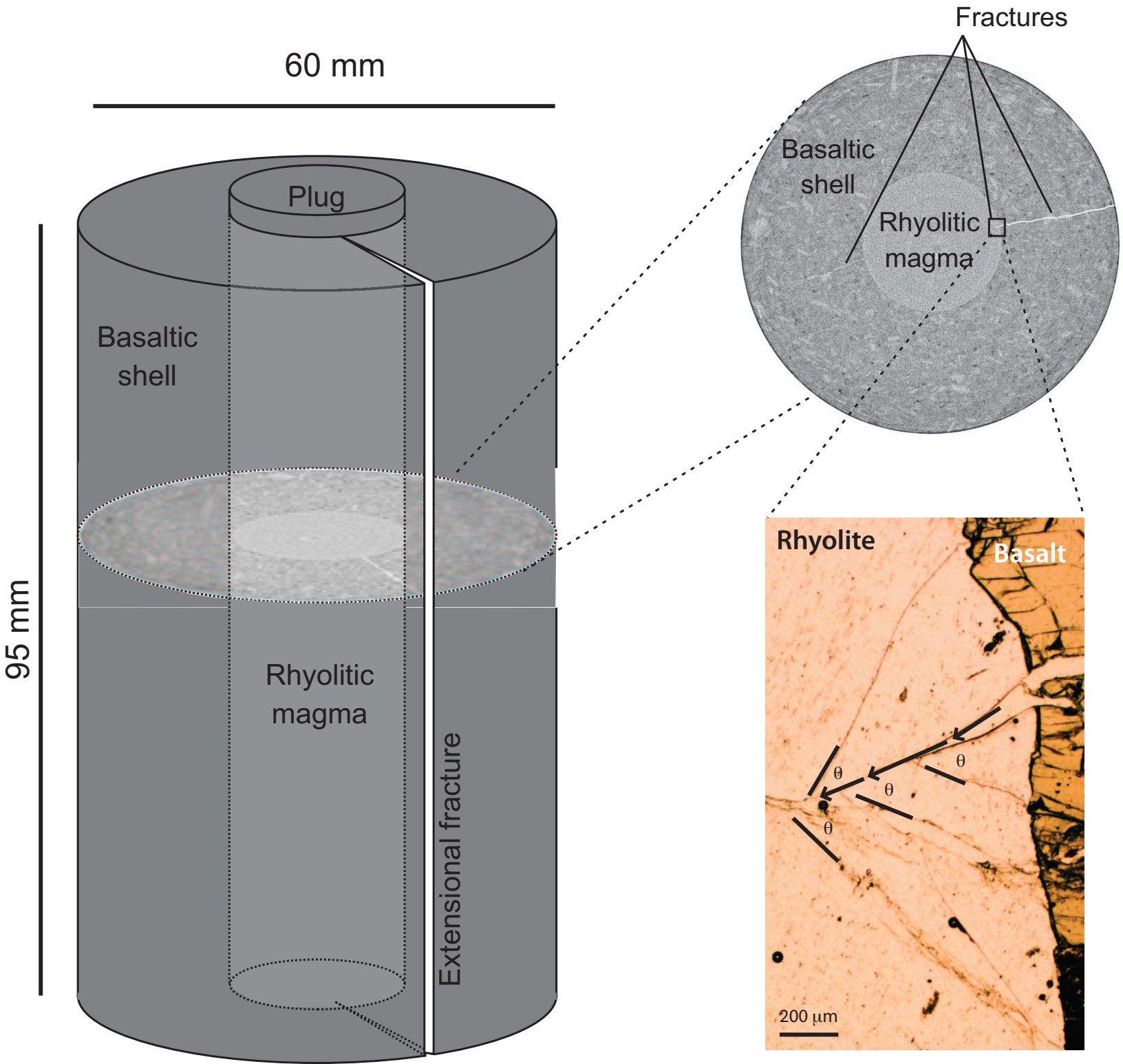

Figure 7.
Click here to download Figure: S_Fig7.eps

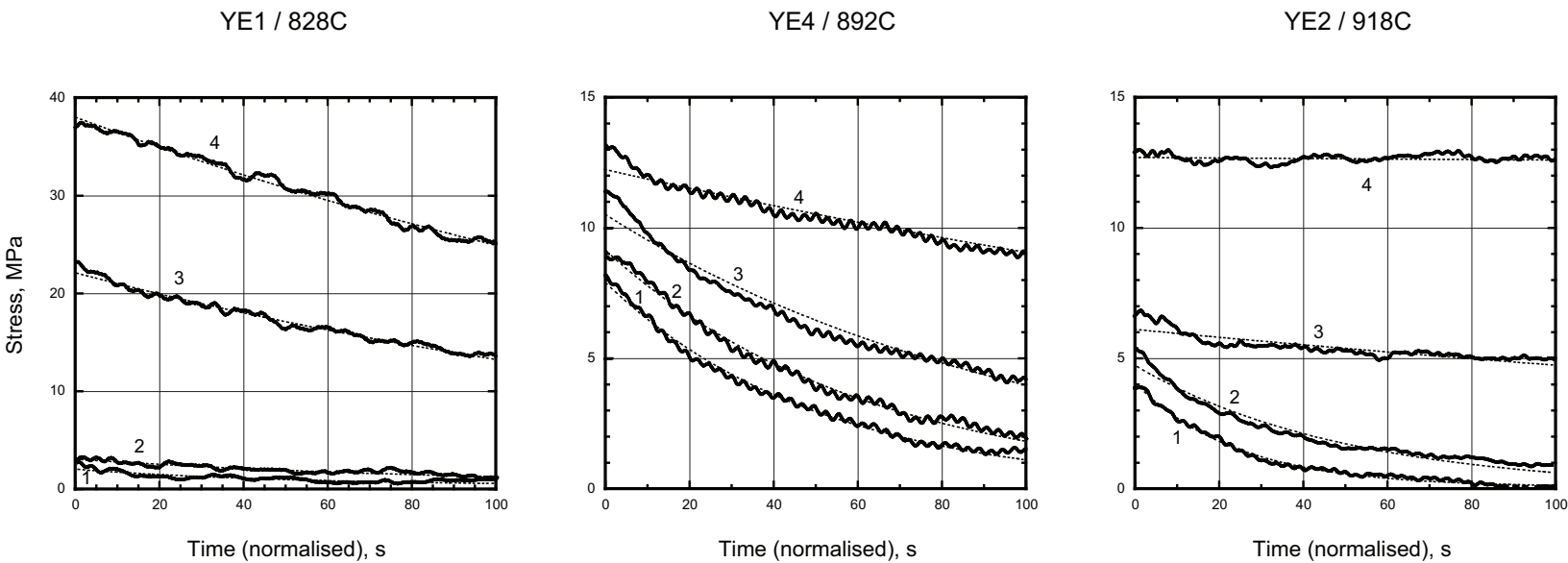

Figure 8.
Click here to download Figure: S_FIG8.eps

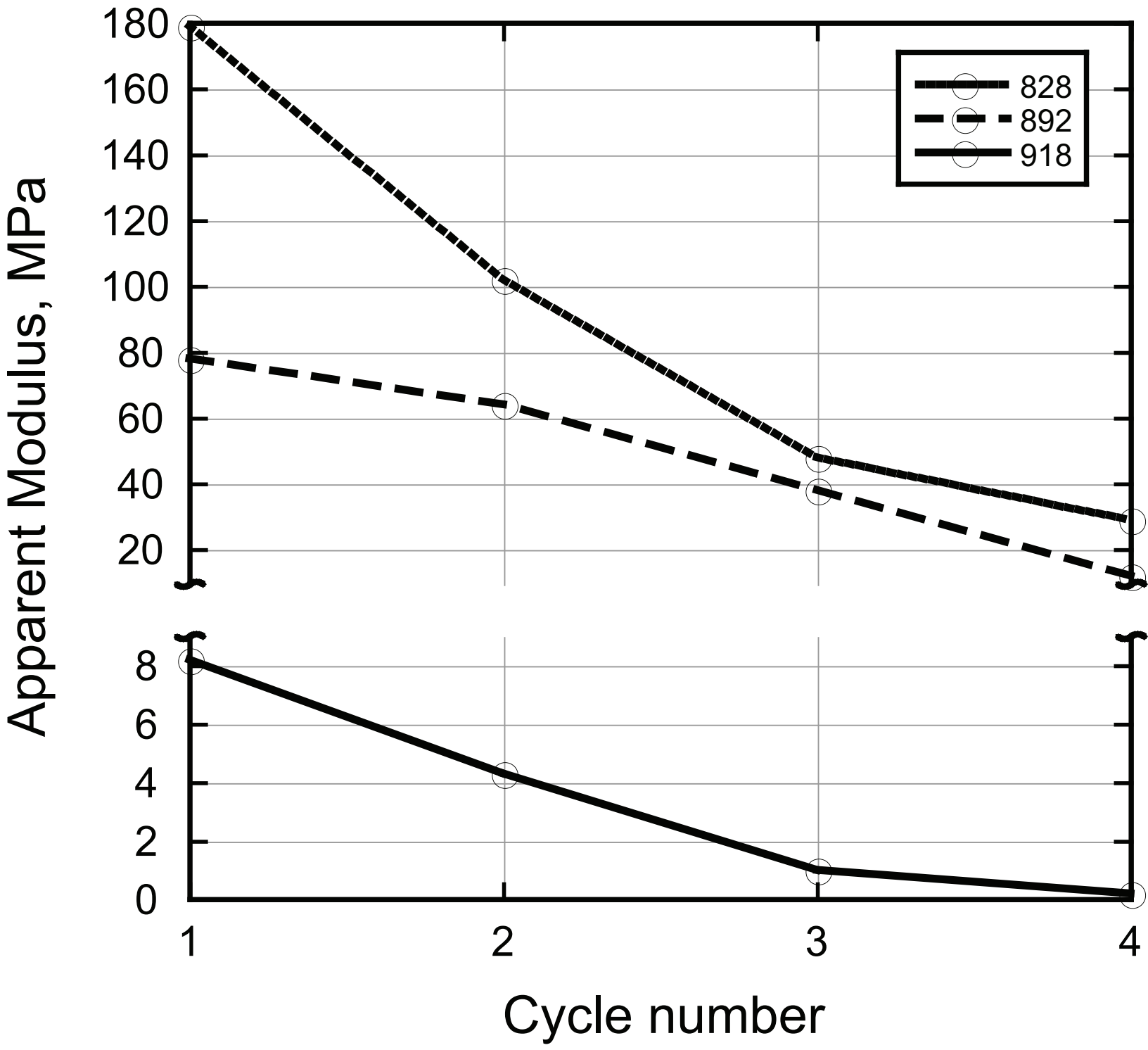

Figure 9.
Click here to download Figure: S_FIG9.eps

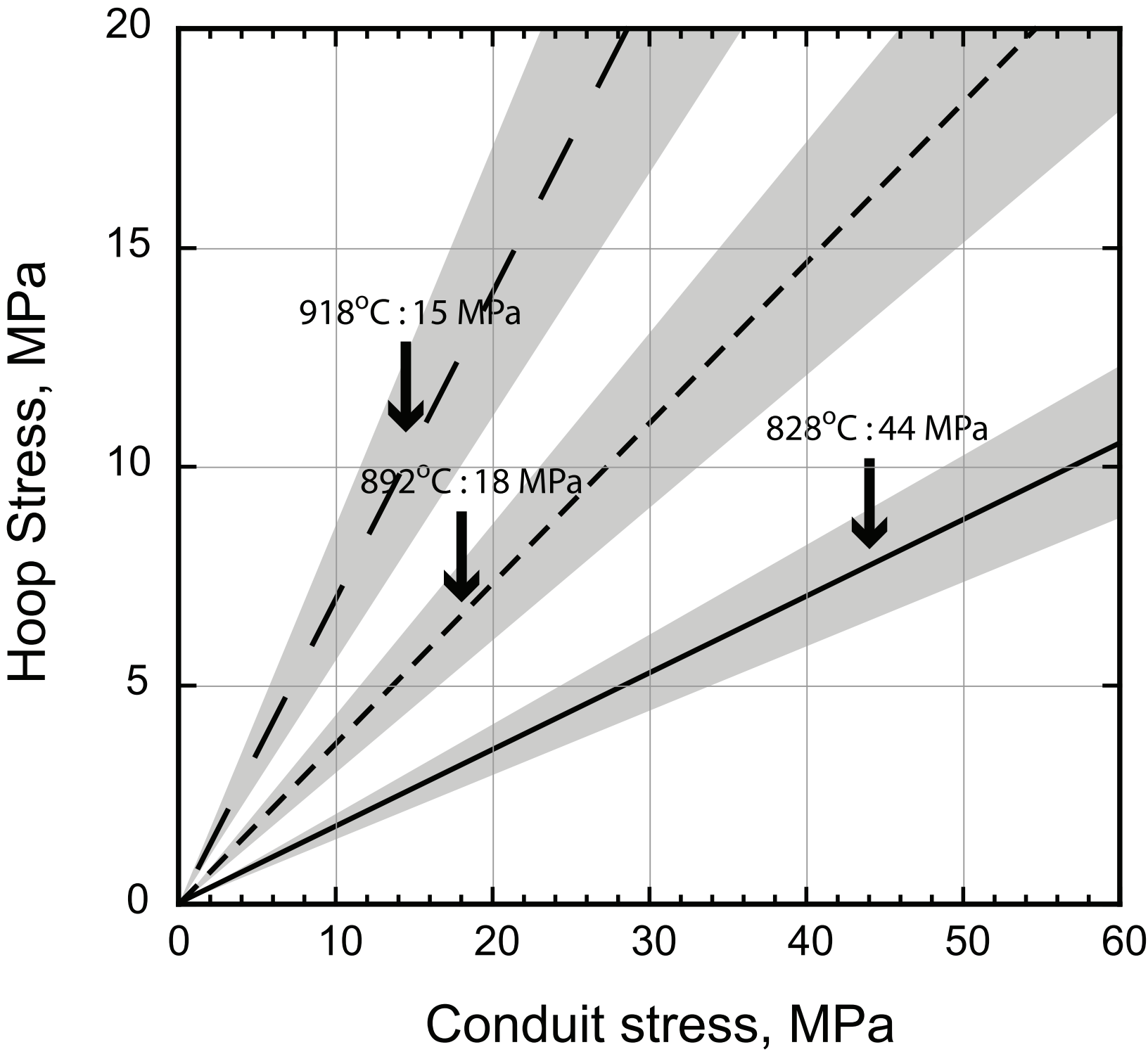

Table 1

Click here to download Table: Table 1.eps

Sample / Temperature, °C	YE1 / 828	YE4 / 892	YE2 / 918
Poissons ratio, ν_{EB}	0.2	0.2	0.2
Poissons ratio, ν_{CO}	0.3/0.35/0.4	0.3/0.35/0.4	0.3/0.35/0.4
Melt viscosity, log unit	8.3	9.6	10.0
M_{EB}, MPa	30	30	30